Title

Diverse contribution of amniogenic somatopleural cells to cardiovascular development: With special reference to thyroid vasculature

Authors

Haneda, Yuka
Miyagawa-Tomita, Sachiko
Uchijima, Yasunobu
et al.

Publication Date

2022-08-29

DOI

10.1002/dvdy.532

Peer reviewed

RESEARCH ARTICLE

Dev Dynamics
DOI10.1002/dvdy.532

Diverse contribution of amniogenic somatopleural cells to cardiovascular development: with special reference to thyroid vasculature

Yuka Haneda [1], Sachiko Miyagawa-Tomita [1, 2], Yasunobu Uchijima [1], Akiyasu Iwase [1], Rieko Asai [1,3], Takahide Kohro [4], Youichiro Wada [5], Hiroki Kurihara [1]

[1] Department of Physiological Chemistry and Metabolism, Graduate School of Medicine, the University of Tokyo, 7-3-1 Hongo, Bunkyo-ku, Tokyo 113-0033, Japan
[2] Department of Animal Nursing Science, Yamazaki University of Animal Health Technology, 4-7-2 Minami-Osawa, Hachioji, Tokyo 192-0364, Japan
[3] Cardiovascular Research Institute, University of California San Francisco, 555 Mission Bay Boulevard South, San Francisco, CA, 94143, USA
[4] Department of Medical Informatics, Jichi Medical University, 3311-1 Yakushiji, Shimotsuke, Tochigi, 329-0498, Japan
[5] Isotope Science Center, The University of Tokyo, 2-11-16, Yayoi, Bunkyo-ku, Tokyo, 113-0032, Japan

*Correspondence: Hiroki Kurihara (e-mail: kuri-tky@umin.net)

Running title: Amniogenic cells in cardiovascular and thyroid development

Present address: Yuka Haneda, Department of Molecular Pathophysiology, Institute for Advanced Medical Sciences, Nippon Medical School, 1-1-5 Sendagi, Bunkyo-ku, Tokyo, 113-8602, Japan.

Grant support:
JSPS KAKENHI Grant Numbers 20J11793, 21K19519, 19H01048, 19K08308, 22H04991 and 22K07877

Keywords:
Amniogenic somatopleure, Quail-chick chimera, Cardiovascular development, Thyroid development, Angiogenesis, FGF, VEGF

Received: Apr 29, 2022;Revised: Aug 23, 2022;Accepted: Aug 23, 2022

Developmental Dynamics

Abstract

Background: The somatopleure serves as the primordium of the amnion, an extraembryonic membrane surrounding the embryo. Recently, we have reported that amniogenic somatopleural cells (ASCs) not only form the amnion but also migrate into the embryo and differentiate into cardiomyocytes and vascular endothelial cells. However, detailed differentiation processes and final distributions of these intra-embryonic amniogenic somatopleural cells (hereafter referred to as iASCs) remain largely unknown.

Results: By quail-chick chimera analysis, we here show that iASCs differentiate into various cell types including cardiomyocytes, smooth muscle cells, cardiac interstitial cells, and vascular endothelial cells. In the pharyngeal region, they distribute selectively into the thyroid gland and differentiate into vascular endothelial cells to form intra-thyroid vasculature. Explant culture experiments indicated sequential requirement of FGF and VEGF signaling for endothelial differentiation of iASCs. Single-cell transcriptome analysis further revealed heterogeneity and the presence of hemangioblast-like cell population within ASCs, with a switch from FGF to VEGF receptor gene expression.

Conclusion: The present study demonstrates novel roles of amniogenic somatopleural cells especially in heart and thyroid development. It will provide a novel clue for understanding the cardiovascular development of amniotes from embryological and evolutionary perspectives.

Introduction

We mammals, avians and reptiles are classified as amniotes because of having the "amnion", a unique extraembryonic membrane that protects the developing embryo from harsh land environment[1,2]. The amnion provides embryos with an aquatic environment to adapt to terrestrial habitats. Therefore, the acquisition of an amniotic membrane has been considered to be one of the most important events of evolution[1,3]. In addition, accumulating evidence has shown that the amnion contains mesenchymal stem-like cells with high plasticity[4–7]. Despite the fact that the amnion is an avascular tissue, amniotic cells are able to differentiate into endothelial cells or cardiomyocytes under a certain condition[8–10]. Due to easy availability without ethical issues and low incidence of rejection even if human amniotic cells are transplanted to another person, effective use of the human amnion for regenerative medicine has been expected[11–14]. However, the normal fate of these cells in the process of amnion development remains unclear.

The amniotic membrane consists of two layers of the ectoderm and the mesoderm origin, although its forming process differs depending on the species[4,15]. In chick embryos, the generation of the amnion occurs after gastrulation, with the appearance of the extraembryonic coelomic cavity in the extraembryonic mesoderm at head fold stage[16–18]. The coelomic cavity separates the lateral mesoderm into two components, somatic and splanchnic mesoderm. The somatic mesoderm forms the somatopleure with the ectoderm, whereas the splanchnic mesoderm forms the splanchnopleure with the endoderm. A large part of the coelomic cavity comes to be extraembryonic, while its most proximal part is marked off by a series of folding processes to give rise to the embryonic body[16–18]. After the headfold stage, the subduction of the embryo causes the extraembryonic part of the somatopleure to cover from above, and finally the membrane closest to the embryo becomes the amnion and the outside becomes the chorion[3]. However, the behavior of this amniogenic somatopleural cell (ASC) population was

unclear because the boundaries between the inside and outside of the embryo at this time were anatomically ambiguous. Therefore, it was not clear whether the ASCs constitute only the extraembryonic membranes (amnion and chorion) or are also involved in the embryonic composition.

In our previous study using chick and quail embryos, we found that ASCs close to the embryonic body not only contribute to the amnion but also migrate into the embryo and differentiate into endothelial cells and cardiomyocytes in the cardiac outflow tract[16]. FGF and BMP signals were suggested to be involved in the differentiation of ASCs into endothelial cells and cardiomyocytes, respectively[16]. However, their intraembryonic distribution and fates have not been fully explored. It remains also unclear which cell population within ASCs is responsive to these signals and what kind of developmental processes take place under different cellular environments.

To address these issues, we first performed quail-chick chimera experiments to trace ASCs entering the embryo (hereafter referred to as 'intra-embryonic ASCs; iASCs') until late embryonic stages. iASCs were distributed to the cardiac outflow tract, where they differentiate into various cell types including cardiomyocytes, vascular endothelial and smooth muscle cells, and interstitial cells. They also distributed to the pharyngeal region, where they contribute to vasculature in the thyroid gland and infrahyoid muscles. Explant culture experiments indicated that a FGF-VEGF signaling relay may drive differentiation of iASCs into vascular endothelial cells. Single-cell (sc) RNA-seq analysis further revealed heterogeneity and the presence of hemangioblast-like cell population within ASCs, with transcriptomic profiles consistent with a switch from FGF to VEGF signaling. Taken together with previous findings, the present study provides new perspectives on cardiopharyngeal development by revealing a novel cardiovascular cell origin and the embryological and evolutionary implications of amniogenesis.

Results

iASCs are widely destined to cervical and thoracic tissues and organs

Here, we performed quail-chick chimera experiments to analyze in detail the distribution of iASCs to embryonic tissues and organs at the late stages, when the major organ primordia are almost complete and start to mature. The quail AS grafts at Hamburger and Hamilton stage (HH)[19] 10 wild-type (WT) or mCherry transgenic embryo (referred to as chFP)[20] were orthotopically transplanted into WT chick AS regions at HH10 to generate quail-chick chimeras (AS chimeras). After 8-day incubation, quail-derived iASCs were detected by quail cell marker antibody (QCPN)[21] or mCherry immunohistochemistry. We analyzed 22 chimeras at HH34-35 (embryonic day 8-9; E8-9), and 5 of them were confirmed intraembryonic contributions of ASCs.

Consistent with the previous study[16], iASCs were observed in the outflow tract of the heart. In the aortic valve, QCPN-positive iASCs were distributed in the valvar interstitium, rather than in the innermost endothelial cell layer as shown Fig. 1B. Near the aortic valve, iASCs were also distributed in the myocardial sheath and the interventricular septum (Fig. 1C and D), where some iASCs were co-stained with MF20, a cardiomyocyte marker but others were not (Fig. 1E-H). Interestingly, iASC distribution was largely restricted to the right ventricle. Furthermore, some iASCs existed around the coronary septal branch and co-stained with monoclonal antibody reactive with smooth muscle α-actin (αSMA), indicating that they differentiated into coronary artery smooth muscle cells (Fig. 1I-L). Thus, iASCs differentiated into not only vascular endothelial cells and cardiomyocytes but also more diverse cell types including vascular smooth muscle cells.

Previously, we have reported that some iASCs are localized to the pharyngeal region, where they are incorporated into vessel walls[16]. To further examine the destination and fates of iASCs in the pharyngeal region, we explored the pharyngeal-arch derived cervical region

of the AS chimeras at late developmental stages. As a result, we observed that iASCs were not evenly distributed within this region, but were rather restricted to specific tissues and organs. In particular, iASCs were concentrated in the infrahyoid muscles (Fig. 1M and N) and the thyroid gland (Fig. 1S and T). The infrahyoid muscles are external laryngeal and tracheal muscles[22], which are particularly well developed in singing birds[23]. In the AS chimeras, both QH1-positive and -negative iASCs existed in the infrahyoid muscles (Fig. 1O-R).

With regard to the avian thyroid gland, there are two independent lobes on the left and right sides without fusing with the parathyroid gland[18,24–26]. In the AS chimeras, thyroid follicular cells were characterized by the expression of thyroid transcription factor-1 (TTF-1), whereas iASCs were distributed in the TTF1-negative interstitium and expressed QH1 (Fig. 1U-X). From the cellular morphology of QH1-positive iASC, it appeared to be integrated into the thyroid vascular network. From the cellular morphology of QH1-positive iASCs, it appeared to be integrated into the thyroid vascular network.

In sum, iASCs differentiate into various cardiovascular cell types, including cardiomyocytes, vascular smooth muscle cells and vascular endothelial cells, depending on the tissue environment.

iASCs contribute to intra-organic vascularization in the thyroid gland

The thyroid gland is a conserved organ in vertebrates and produces hormones that are important for maintaining homeostasis[27]. However, the details of its developmental process have not been fully clarified. In avians, the thyroid gland is derived from the endodermal floor of the pharynx through a process consisting of five stages: specification, budding, descent, bilobation and folliculogenesis[28,29]. The vasculature of the thyroid gland develops at approximately HH27 (E5), just after the bilobation stage[18]. To elucidate when iASCs are

distributed into the thyroid, we performed immunohistochemistry of mCherry as well as QH1 in mCherry-positive chimeras at HH27, HH30 (E6.5) and HH32 (E7.5). At HH27, QH1-positive iASCs were observed to be incorporated into blood vessels around the thyroid anlage visualized by ink injection (Fig. 2A-D, arrowheads). At HH30, blood vessels were found in the thyroid, indicating that vascular invasion starts between HH27 and HH30 (Fig. 2E-H). At HH32, mCherry-positive iASCs were abundantly distributed in the thyroid, most of which were positive for QH1 (Fig. 2I-L). These results indicate that iASCs are incorporated into perithyroid blood vessels through vasculogenesis before HH27 and migrate into the thyroid as angiogenic endothelial cells between HH25 and HH32.

FGF and signals from the thyroid gland are required for vascularization by ASCs

Then we focused on the selective incorporation of iASCs into the thyroid vasculature to clarify the underlying mechanisms. To investigate whether the incorporation of iASCs into the thyroid vasculature required signals from the thyroid gland, quail ASCs at HH10 were co-cultured with the chick thyroid anlage at HH30. For comparison, ASCs were also co-cultured with clumps including the thymus and parathyroid gland (Fig. 3A). However, QH1-expressing cells did not appear under either condition (Fig. 3B a, b, e and f).

In the previous study, we revealed that FGF signaling from the pharyngeal mesenchyme is important for AS to endothelial differentiation[16]. Therefore, the same experiments were performed in the presence of FGF2. As a result, many QH1-expressing cells appeared from ASCs around the chick thyroid anlage at HH30, forming a sheet-like structure (Fig. 3B c and d). By contrast, only a few QH1-expressing cells were observed in co-culture with the clumps including the thymus and parathyroid gland despite the presence of FGF2 (Fig. 3B g and h). The same results were obtained when quail ASCs were co-cultured with HH35 (E9) chick

organs (Fig. 3C and D). These results indicate that both FGF and thyroid-derived signals are required for endothelial differentiation of ASCs.

It is known that the thyroid hormone thyroxine starts to accumulate from HH10 and increases logarithmically until HH20 (E3)[28]. To investigate whether thyroxine is involved in vascular endothelial differentiation, we cultured ASCs with thyroxine. However, no QH1 expression was observed without or with FGF2, indicating that the endothelial differentiation of ASCs was independent of the hormone-secreting function of the thyroid (data not shown).

Sequential FGF and VEGF signaling promotes vascular endothelial differentiation of ASCs

A previous study using mice reported that thyroid parenchymal cells express *VEGF-A* and the surrounding *KDR*/*VEGFR2*-expressing cells differentiate into vascular endothelium[30]. Indeed, the expression level of *VEGF-A* was higher in the thyroid gland than in the surrounding organs also in chickens (Fig. 4A). These results led us to the idea that FGF signals from the pharyngeal mesenchyme and VEGF from the thyroid parenchyma may sequentially cooperate to promote endothelial differentiation of ASCs. Indeed, the expression of the major VEGF receptor *KDR*/*VEGFR2* was found to be upregulated by FGF2 with a peak around 24 hours after treatment (Fig. 4B). Furthermore, in vitro AS culture experiments showed that sequential treatment with FGF2 and VEGF-A for 24 hours each (FGF2 24h + VEGF 24h) significantly increased the number of QH1-positive cells in cultured quail ASCs (Fig. 4C). QH1-positive cells typically constituted plexiform sheet-like structure expanding from AS explants, which were not induced to form by FGF or VEGF treatment alone, although sporadic QH1-positive cells were found in these conditions. This suggests that FGF2 may drive ASCs into a state similar to *KDR*/*VEGFR2*-expressing cells that differentiate various cell types including cardiovascular cells and hematopoietic cells[31].

To further characterize the nature of QH1-positive cells, we investigated expression levels of vascular endothelium-related genes (undifferentiated endothelial and hematopoietic markers *KDR*/*VEGFR2*, *TAL1* and *LMO2*, and mature vascular endothelial marker *CDH5*)[32–34] in the absence or presence of FGF2 and/or VEGF-A. As a result, the expression levels of these markers were significantly upregulated in the group of FGF2 24h + VEGF 24h compared to other groups (Fig. 5A-D), suggesting that FGF signals stimulate *KDR*/*VEGFR2* expression and subsequent VEGF signals promote vascular endothelial differentiation of ASCs. We also noticed that the expression levels of FGF receptors were significantly reduced in ASCs as endothelial differentiation progressed (Fig. 5E-G). These results suggest that FGF works in the early stage of vascular endothelial differentiation.

To investigate whether vascular endothelial differentiation potentials of ASCs are dependent on developmental stages, the grafts of quail amniotic membrane at HH30 were cultured under specific conditions. In contrast to ASCs at HH10, amniotic grafts at HH30 did not yield QH1-positive cells even in the presence of both FGF and VEGF signaling (Fig. 6). This result indicates that vascular endothelial differentiation potentials in response to FGF and VEGF signals are restricted to ASCs at early embryonic stages and disappear in mature amniotic cells, consistent with previous studies showing that mesodermal cells have differentiated into smooth muscle cells in the amniotic membrane by around HH27[35–37].

Single-cell transcriptome analysis identifies endothelial progenitor-like ASCs before intraembryonic translocation

To further investigate the heterogeneity of ASCs or iASCs *in vivo*, single-cell RNA sequencing (scRNAseq) was performed using the Fluidigm C1 system. First, we collected ASCs from HH10 chick which included cells of ectoderm and somatic mesoderm origins (Fig. 7A). After quality filtering, a dataset comprising 89 ASCs was subjected to further

analysis. To reveal characteristics of ASCs, scRNAseq data of ASCs were mapped on UMAP[38] and cells were divided into 7 clusters (Fig. 7B). Differentially expressed genes between each cluster shown in Fig. 7C and D revealed that clusters 0 and 5 were likely ectodermal cells because they highly expressed the ectoderm or epithelium markers *CDH1* and *EPCAM*[39,40]. Therefore, other clusters are considered to be mesodermal, of which clusters 3 and 4 expressed mesodermal stem-related genes such as *CXCL12* and *CDH11*[41,42]. *ANGPTL1*, a growth factor largely specific for vascular endothelium, was also expressed in these clusters[43]. Cells in cluster 1 were characterized by the expression of some neuronal marker genes such as *CDH2* and *NCAM1*. Of note, cells in cluster 6 had high expression of genes related to vascular endothelial or hematopoietic cells such as *KDR/VEGFR2, CDH5, LMO2*, *PECAM1* and *CD34*. Cells in cluster 2 were regarded as of low quality because of the low number of detected genes (nFeature RNA) excluded from further analysis. Re-embedding with UMAP (Fig. 8A) and velocity analysis[44] (Fig. 8B) again showed ectodermal and mesodermal cluster groups, in the latter of which a flow towards cluster 6. Pseudotime analysis on the mesodermal clusters using Monocle 3[45] (Fig. 8C and D) showed downregulation of FGF receptor gene expressions (Fig. 8Ea-c) and upregulation of VEGF receptor gene expressions (Fig. 8Ed-f) during the putative transition from mesodermal to endothelial cells. These results are consistent with the present *in vitro* experiments showing sequential requirement of FGF and VEGF signaling for ASC differentiation into vascular endothelial cells.

Discussion

Here, we describe that intra-embryonic amniogenic somatopleure cells (iASCs) differentiate into various cell types constituting the cardiovascular system including the thyroid vascular network.

Recent studies have identified three of heart fields (e.g., the first, second, and tertiary heart fields) in intra-embryonic splanchnic mesoderm[46,47]. These cardiogenic mesodermal regions contribute to distinct parts of the heart, and differentiate into lineage-specific various types of cells, including cardiomyocytes and endothelial cells[46–48]. In contrast, iASCs, which arise from the extra-embryonic somatopleure, migrate into the primary heart tube from the outflow tract during amnion formation[16]. Previously, we have proposed a model in which FGF and BMP signaling from pharyngeal and outflow regions may direct iASC differentiation into endothelial cells and cardiomyocytes, respectively, at the outflow tract and right ventricle[16]. The present study revealed that the distribution of iASCs in the interventricular septum at HH34-35 was enriched in the right ventricular side (Fig. 1A-D). This distribution pattern of iASCs is similar to that of the cardiogenic precursor cells derived from the second heart field (SHF)[46,49]. It is an interesting possibility that iASCs may be a previously unrecognized extra-embryonic subpopulation of SHF. However, the expression of ISL1 (a SHF marker [49,50]) was not detected in the AS mesoderm at HH10[16], implying that iASCs are not incorporated in SHF at this stage. Further studies, including lineage analysis of iASCs with SHF markers (such as Isl1 and Fgf10[51,52]) from earlier stages, will clarify the relationship between iASCs and SHF. Although it remains to be determined whether these cell populations represent distinct cell lineages or not, they likely share common behavioral characteristics to contribute to the formation of the outflow tract.

Stimulation of FGF significantly increased *KDR/VEGFR2* expression in ASCs, whereas the expression of *FGFRs* tended to decrease when the differentiation into the vascular

endothelium progressed. This suggests that initial stimulation by FGF signal may act as a trigger for the early stages of vascular endothelial differentiation, and then thyroid-derived signals including VEGF may promote vascular endothelial cell maturation. Vascular invasion into the thyroid had already started at HH27 (Fig. 2E-H), and transplanted quail ASCs (QCPN-positive cells) entered the thyroid and differentiated into QH1-positive vascular endothelial cells (Fig. 1S-X) before HH35, by which differentiation steps involving sequential FGF and VEGF-A signaling are already accomplished. Since VEGF-A is also secreted from the thyroid gland at HH35, differentiation of QH1-positive endothelial cells in the co-culture with quail ASCs seems to recapitulate these processes (Fig. 3C). This FGF-induced endothelial differentiation potential is likely to be lost in the later amniotic mesoderm at HH30 probably because of their commitment to smooth muscle differentiation (Fig. 6)[35–37]. Based on these findings, we propose a model for the differentiation process of iASCs as shown in Fig. 9.

According to scRNAseq, some ASCs express markers of hematopoietic progenitors. Interestingly, it has been reported that hematopoietic foci like blood islands are found in the mesenchyme close to the branchial artery in HH15 chick embryos[53,54]. Recent reports also revealed new hematopoietic sites such as in the endocardium[55–57]. Moreover, Shigeta et. al. demonstrated macrophage differentiation from the hemogenic endocardium and its essential role in valvular remodeling[58], suggesting that the temporary hematopoiesis may be important for tissue remodeling, as well as for supplying circulating blood to the whole body. Although we were unable to show directly that ASCs differentiate into blood cells, it is quite possible that iASC may contribute to hematopoiesis through endothelial differentiation in the cardiac outflow tract and pharyngeal arch regions or directly forming hematopoietic foci.

The process of amnion formation varies greatly among species. Since reptiles and birds diverged from the same ancestor and developed amnion[59], the properties of the amnion of

these two species may be similar. Rather, mammals have acquired novel traits such as retraction of the chorioallantoic membrane and formation of the placenta. Despite these differences, mouse studies have reported that *Flk1* (*KDR/VEGFR2* herein)-expressing cells are present in the amnion[31], and that there are a few cells destined for blood islands and PGCs in the presumptive amnion[60]. Moreover, Zhang *et. al.* recently reported that a part of the extraembryonic mesoderm gives rise to cardiomyocytes and serosal mesothelial cell types[61]. These cells may be considered comparable with iASCs in avians, although the route of entrance into the developing heart appears to be different between arterial and venous poles possibly due to topological differences in the position of the extraembryonic/intraembryonic boundary.

From an evolutionary viewpoint, it is intriguing to pursue whether iASCs contribute to the anatomical and functional diversity among species. The thyroid gland is considered to be evolutionarily derived from the endostyle, an exocrine organ, and the branching structure is a remnant of that[62]. In particular, the morphology and anatomy of the thyroid and associated vessels changes between species[27,63]. Therefore, it is interesting to investigate if the different usage of iASC might be involved in thyroid morphogenesis.

The next challenge is to explore how the AS was acquired in the process of evolution. One fascinating possibility is that some migratory pluripotent cells with a potential to diverse cell types might led to the acquisition of the amniotic membrane, as neural crest cells, pluripotent stem cells with migratory capacity arising in the neural plate border, generated the “new head” as an evolutionary novelty in vertebrates[64]. For this purpose, it is necessary to explore whether there is a homologue of the AS in non-amniotes such as fish and amphibians.

Conclusion

Here, we showed that amniogenic somatopleure cells (ASCs) differentiate into various cell types constituting the cardiovascular system, with some populations having a molecular background similar to that of hemangioblasts. Among them, those contributing to the thyroid vascular network were suggested to differentiate into vascular endothelial cells with FGF-specification and VEGF-induced maturation. This study will provide a novel clue for understanding the cardiovascular development of amniotes from embryological and evolutionary perspectives.

Experimental Procedures

Animals

Fertilized Boris Brown (Gallus gallus, wild type, WT) eggs and Japanese quail (Coturnix japonica, WT) eggs were obtained from Inoue Egg Farm (Kanagawa, Japan) and Motoki Hatchery (Saitama, Japan), independently. PGK:H2B-chFP-TG (chFP) quail eggs[20] were provided by the Avian Bioscience Research Center at Nagoya University as part of the National Bioresources Program. All eggs were incubated at 37 °C in a humid incubator at 37 °C to appropriate embryonic stages. All experiments using animals were reviewed and approved by the University of Tokyo Animal Care and Use Committee and were performed in accordance with the institutional guidelines for care and use of laboratory animals. Staging of chick/quail embryos were according to Hamburger and Hamilton (1951).

Quail-chick chimera

To reveal the distributions of specific cells of interest, quail-chick chimera analysis was performed. Quail-chick chimeras of the AS ("AS chimera") has been described in the previous study[16]. When making AS chimera, HH10 WT or chFP quail AS grafts were transplanted into both right and left regions of the AS of HH10 host chick embryos.

Histological analysis

For histological analyses, AS chimeras and embryos were collected, some of which injected ink (Kiwa-Guro, Sailor, Japan) into the extra-embryonic vitelline vein or into the heart using a glass micropipette to visualize whole blood vessels. Embryos were then fixed with 4% paraformaldehyde (PFA), stored in PBS, embedded in paraffin (Kanto Chemical, Tokyo, Japan).

Immunofluorescence staining of paraffin or frozen sections (10-14 μm) ware performed using following primary antibodies: anti-quail cell (QCPN; DSHB, 1:100), QH1 (DSHB, 1:100), Nkx2.1 (also known as thyroid transcription factor 1 /Titf1) (Biopat, 1:1500), mCherry (SCIGEN, 1:500), MF20 (DSHB, 1:30), and αSMA (1A4-FICT, Sigma, 1:500). Paraffin sections were antigen activated by pH6 citric acid solution and inactivated of endogenous peroxidase with diluted 30% H_2O_2 (Wako, 1:20). Signals were visualized with Alexa Fluor-conjugated secondary antibodies (Abcam, 1:400) specific for the appropriate species. For DAPI staining, diluted DAPI (Sigma-Aldrich, 1/1000) in PBST was applied after all procedures. Some sections were treated with biotin-conjugated secondary antibodies and 3,39-diaminobenzidine (DAB) staining was performed using the Vectastain ABC System (Vector Laboratories). For counterstaining, Mayer's Hematoxylin (Muto pure chemicals, 1:20) and/or diluted Eosin (Muto pure chemicals, 1:50) in 50% EtOH were used.

Images of the immunofluorescence staining were captured using a Nikon C2 confocal microscope. DAB staining was observed under OLYMPUS AX80 motorized microscope. All images were processed using ImageJ and Nikon NIS Elements software.

Explant cultures

The AS graft which included both ectodermal and mesodermal layers were excised from HH10 WT or chFP quail embryos and placed in a gelatin-coated 3.5-cm dish (IWAKI) containing 1%FBS DMEM (Wako) medium at 37 °C in 5% CO2 to appropriate time. In organ culture, the thyroid, parathyroid, and thymus from HH30 or HH35 chick embryos were collected, and co-culture with the quail AS graft. The explants were pasted on the bottom dish with a glass needle or fine forceps before incubation. When the cut out HH10 quail AS tissue which contained both ectodermal and mesodermal layer was cultured on the gelatin coated dish, the ectodermal cells became shrunk and mesodermal cells expanded radially. In

some experiments, L-thyroxine (Nacalai, 100nmol/L), rm-bFGF (FGF2) (233-FB, R&D, 20 ng/ml) and VEGF (293-VE, R&D, 50ng/ml) were added in the culture medium (1% FBS in DMEM). The concentration of each additive was determined after preliminary experiments based on previous reports. For control, an appropriate amount of vehicle was added in the culture medium.

For immunocytochemistry, cells were fixed with 4% PFA for 10 min. After washing with PBS, cells were immunoreacted with first antibodies for overnight and secondary antibodies for 2 hours and stained with DAPI solution as described in histological analysis. Images of the immunofluorescence staining were captured using a Keyence BZ-X700 microscope.

The explant cell areas and QH1 positive areas were quantified after binarizing the images with ImageJ software. All ectodermal regions or the part where the grafts overlapped to form a thick cell layer were excluded from analysis.

RNA extraction and qRT-PCR (qPCR)

For RNA extraction from cultured quail ASCs, the cells were washed with PBS to remove medium and lysed with ISOGEN2 (500 µL, Wako). After lysing cells, total RNA was obtained following the manufacturing procedure. The RNA concentration was determined at 260 nm by SimpliNano. The total RNA was reverse transcribed following the ReverTra Ace® qPCR RT Kit (Toyobo) procedure. The primers used for qPCR are listed in Table S1. For primers of quail *GAPDH, VEGFR2* and *TAL1* were referred to Giles et. al. 2005[65] and qual *CDH5* was referred to Yvernogeau et. al. 2016[66]. Other primers were designed by Primer-Blast (https://www.ncbi.nlm.nih.gov/tools/primer-blast/) or Primer3Plus (https://www.bioinformatics.nl/cgi-bin/primer3plus/primer3plus.cgi). PCR was performed on GeneAmp® PCR SYSTEM 9700 (Applied Biosystems). qPCR was performed using the LightCycler 480 (Roche) real-time system according to the manufacturer's instructions. To

reduce errors when applying to 96well plates, duplicate samples were created. Absolute quantification was performed using the second derivative max method with the number of cycles of the maximum value when the amplified signal was differentiated twice as the cross point (Cp). Then, the concentration was calculated from the standard curve and the value divided by the GAPDH value was compared. The value of concentration of duplicated samples were averaged. All experiments were performed in parallel and repeated three or more independently.

Single-cell RNA sequencing

- *Cell preparation*

For ASCs single-cell preparation, AS grafts including ectodermal and mesodermal layers were collected from more than 15 chick embryos at HH10 (referred to as st10 or E1.5 in the dataset). The grafts were treated with 0.25 w/v% trypsin/EDTA (0.2g/L) at 37 ℃, 15 min to dissociate into single cells. Enzymes were neutralized with equal volume of DMEM with 10% fetal bovine serum (FBS). Cell suspensions were filtered through a 35-μm nylon mesh cell strainer (FALCON, 352235) to exclude debris and cell clumps.

- *mRNA sequencing*

Prepared cells were captured on the Fluidigm C1 Single-Cell Auto Prep Array integrated fluidic circuit (IFC) for small cells (5-10 μm in diameter). Cells were loaded on the IFC chips at concentration of 500 cells per μL. All captured cells were photographed to check if they were truly dissociated for single cells by using KEYENCE BZ-X710. cDNAs of captured single cells were prepared by using SMARTer v4 Ultra Input Low RNA kit for the Fluidigm C1 System (Clontech). Then cDNAs were quality checked by using the Agilent 2200 TapeStation system and quantified by Qubit (Thermo Fisher). High quality cDNAs were

further constructed sequencing libraries by using Nextera XT DNA Sample Preparation Kit (Illumina). Each single-cell cDNAs were sequenced 50 pair-end on the Illumina Hiseq 2500.

- *Data analysis*

Data analysis was performed in R version 3.6.0 and Python 3.7. All graphical figures were created by the ggplot2 R package. Sequence output fastq files were aligned to chick ensemble genome reference (Gallus_gallus.GRCg6a.96) with extra GFP and spike DNA sequences by using HISAT2 software version 2.1.0. Gene expression counts were calculated with the featureCounts function from the Rsubread version 1.34.7 package using R. All scRNA-seq data have 123 ASCs.

The gene name was converted from chick Ensembl ID to gene symbol, and duplicated genes integrated as Ensembl ID to use for further analysis. Each count data was converted into a Seurat object by using Seurat version 4.0.4 R package[67].

HH10 ASCs were normalized using 89 cells of number of feature RNA > 2000. For cell clustering, the 2-dimensional UMAP space was used[38]. Each differentially expressed genes (DEGs) corresponding to each cluster were calculated by using FindAllMarkers function. The statistical significance was performed with a Wilcoxon Rank Sum test and the threshold was limited by log2 fold change was more than 0.25. For Fig. 7C, the heatmap was created by using DoHeatmap function and the colour indicates z-scored expression values in each cell.

RNA velocity analysis[44] was performed by using velocyto, including velocyto.py version 0.17.17 Python package and velocyto.R version 0.6. The expression counts of each spliced and unspliced genes were calculated through mapping to chick genome reference (Gallus_gallus.GRCg6a.96) by using run_smartseq2 function from velocyto.py. Then, RunVelocity and show.velocity.on.embedding.cor function in SeuratWrappers version 0.1.0 package in R were used for the visualization of RNA velocity on the UMAP space. From the

direction of RNA velocity, each sub trajectory of pseudotime was calculated by using monocle3 version 0.1.1 R package. This was used for the visualization of transition of gene expression patterns along with pseudotime.

The dataset is available at the NCBI Gene Expression Omnibus, under accession GSE201285.

Statistical analysis

For Fig. 3D and Fig. 4D, P values were determined by ANOVA with Tukey–Kramer's post hoc test. *P*-values <0.05 were considered statistically significant. For Fig. 5A-D, the Kruskal–Wallis test as a nonparametric method was used to compare mean values, followed by the Mann–Whitney U-test. R environment (Rstudio, Inc., Boston, USA) was used. *P*-values <0.0125 were considered statistically significant. For Fig. 4A and Fig. 5E-H, Welch's *t*-test for unequal variances was performed after the normality of the data was confirmed using the Shapiro–Wilk normality test ($\alpha = 0.05$). *P*-values <0.05 were considered statistically significant. Data were obtained from three or more independent experiments.

Author contribution

Y.H., S.M.-T, R.A. and H.K conceived the project and designed the experiments and wrote the manuscript. Y.H. and S.M.-T. performed experiments. Y.H., Y.U., A.I., K.T. and S.M.-T. analyzed data. Y.W. provided instruments. Y.H., S.M.-T, R.A. and H.K wrote the manuscript with contributions from all of the authors.

Acknowledgments

We thank Rusty Lansford (Keck School of Medicine of USC) and Yuki Sato (Kyushu University) for providing the mCherry-transgenic Japanese quail line; Hiroaki Nagao and Kenji Yoshihara (Tokyo Women's Medical University) for their technical support; Dr. Hiroyuki Aburatani, Dr. Shiro Fukuda, Dr. Shogo Yamamoto (RCAST, University of Tokyo) and Akashi Taguchi (ISC, University of Tokyo) for scRNA-seq data analysis. We also thank all of the laboratory members for their helpful discussion and encouragement.

This work was supported in part by JSPS KAKENHI Grant Numbers 20J11793 (Y.H.), 21K19519, 19H01048 and 22H04991 (H.K.), 19K08308 and 22K07877 (S. M.-T.) and a stipend from the World-leading Innovative Graduate Study Program for Life Science and Technology (WINGS-LST) (Y.H.).

References

1. Ferner K, Mess A. Evolution and development of fetal membranes and placentation in amniote vertebrates. *Respir Physiol Neurobiol*. 2011;178(1):39-50. doi:10.1016/j.resp.2011.03.029

2. Starck JM, Stewart JR, Blackburn DG. Phylogeny and evolutionary history of the amniote egg. *J Morphol*. 2021;282(7):1080-1122. doi:10.1002/jmor.21380

3. de Melo Bernardo A, Chuva de Sousa Lopes SM. The involvement of the proamnion in the development of the anterior amnion fold in the chicken. *PLoS One*. 2014;9(3):e92672. doi:10.1371/journal.pone.0092672

4. Dobreva MP, Pereira PNG, Deprest J, Zwijsen A. On the origin of amniotic stem cells: of mice and men. *Int J Dev Biol*. 2010;54(5):761-777. doi:10.1387/ijdb.092935md

5. Miki T, Lehmann T, Cai H, Stolz DB, Strom SC. Stem cell characteristics of amniotic epithelial cells. *Stem Cells*. 2005;23(10):1549-1559. doi:10.1634/stemcells.2004-0357

6. Miki T, Mitamura K, Ross MA, Stolz DB, Strom SC. Identification of stem cell marker-positive cells by immunofluorescence in term human amnion. *J Reprod Immunol*. 2007;75(2):91-96. doi:10.1016/j.jri.2007.03.017

7. Seo MS, Park SB, Kim HS, Kang JG, Chae JS, Kang KS. Isolation and characterization of equine amniotic membrane-derived mesenchymal stem cells. *J Vet Sci*.

2013;14(2):151-159. doi:10.4142/jvs.2013.14.2.151

8. Koob TJ, Lim JJ, Massee M, et al. Angiogenic properties of dehydrated human amnion/chorion allografts: therapeutic potential for soft tissue repair and regeneration. *Vasc Cell*. 2014;6:10. doi:10.1186/2045-824X-6-10

9. Ginsberg M, James D, Ding BS, et al. Efficient direct reprogramming of mature amniotic cells into endothelial cells by ETS factors and TGFβ suppression. *Cell*. 2012;151(3):559-575. doi:10.1016/j.cell.2012.09.032

10. Zhao P, Ise H, Hongo M, Ota M, Konishi I, Nikaido T. Human amniotic mesenchymal cells have some characteristics of cardiomyocytes. *Transplantation*. 2005;79(5):528-535. doi:10.1097/01.tp.0000149503.92433.39

11. Toda A, Okabe M, Yoshida T, Nikaido T. The Potential of Amniotic Membrane/Amnion-Derived Cells for Regeneration of Various Tissues. *J Pharmacol Sci*. 2007;105(3):215-228. doi:10.1254/jphs.CR0070034

12. Nakamura T, Inatomi T, Sotozono C, Amemiya T, Kanamura N, Kinoshita S. Transplantation of cultivated autologous oral mucosal epithelial cells in patients with severe ocular surface disorders. *Br J Ophthalmol*. 2004;88(10):1280-1284. doi:10.1136/bjo.2003.038497

13. Kinoshita S, Nakamura T. Development of cultivated mucosal epithelial sheet transplantation for ocular surface reconstruction. *Artif Organs*. 2004;28(1):22-27. doi:10.1111/j.1525-1594.2004.07319.x

14. Umezawa A, Hasegawa A, Inoue M, et al. Amnion-derived cells as a reliable resource for next-generation regenerative medicine. *Placenta*. 2019;84:50-56. doi:10.1016/j.placenta.2019.06.381

15. Pereira PNG, Dobreva MP, Graham L, Huylebroeck D, Lawson KA, Zwijsen AN. Amnion formation in the mouse embryo: the single amniochorionic fold model. *BMC Dev Biol*. 2011;11:48. doi:10.1186/1471-213X-11-48

16. Asai R, Haneda Y, Seya D, et al. Amniogenic somatopleure: a novel origin of multiple cell lineages contributing to the cardiovascular system. *Sci Rep*. 2017;7(1):1-14. doi:10.1038/s41598-017-08305-2

17. Patten Bradley M (Bradley Merrill). The early embryology of the chick. Published online 1920:192. https://www.biodiversitylibrary.org/bibliography/23947

18. Romanoff, Lawrence A. *The Avian Embryo, Structural and Functional Development*. Macmillan; 1960. https://www.worldcat.org/title/avian-embryo-structural-and-functional-development/oclc/561075

19. Hamburger V, Hamilton HL. A series of normal stages in the development of the chick embryo. *J Morphol*. 1951;88(1):49-92. https://www.ncbi.nlm.nih.gov/pubmed/24539719

20. Huss D, Benazeraf B, Wallingford A, et al. A transgenic quail model that enables dynamic imaging of amniote embryogenesis. *Development*. 2015;142(16):2850-2859. doi:10.1242/dev.121392

21. Selleck MA, Bronner-Fraser M. Origins of the avian neural crest: the role of neural plate-epidermal interactions. *Development*. 1995;121(2):525-538. https://www.ncbi.nlm.nih.gov/pubmed/7768190

22. Huang R, Zhi Q, Izpisua-Belmonte JC, Christ B, Patel K. Origin and development of the avian tongue muscles. *Anat Embryol* . 1999;200(2):137-152. doi:10.1007/s004290050268

23. Larsen ON, Goller F. Direct observation of syringeal muscle function in songbirds and a parrot. *J Exp Biol*. 2002;205(Pt 1):25-35. https://www.ncbi.nlm.nih.gov/pubmed/11818409

24. Abdel-Magied EM, King AS. The topographical anatomy and blood supply of the carotid body region of the domestic fowl. *J Anat*. 1978;126(Pt 3):535-546. https://www.ncbi.nlm.nih.gov/pubmed/689991

25. Kameda Y. Morphological and molecular evolution of the ultimobranchial gland of nonmammalian vertebrates, with special reference to the chicken C cells. *Dev Dyn*. 2017;246(10):719-739. doi:10.1002/dvdy.24534

26. Hilfer SR, Brown JW. The development of pharyngeal endocrine organs in mouse and chick embryos. *Scan Electron Microsc*. 1984;(Pt 4):2009-2022. https://www.ncbi.nlm.nih.gov/pubmed/6523066

27. Nilsson M, Fagman H. Development of the thyroid gland. *Development*. 2017;144(12):2123-2140. doi:10.1242/dev.145615

28. Shain WG, Hilfer SR, Fonte VG. Early organogenesis of the embryonic chick thyroid: I. Morphology and biochemistry. *Dev Biol*. 1972;28(1):202-218. doi:10.1016/0012-1606(72)90138-8

29. Maeda K, Asai R, Maruyama K, et al. Postotic and preotic cranial neural crest cells differently contribute to thyroid development. *Dev Biol*. 2016;409(1):72-83. doi:10.1016/j.ydbio.2015.10.026

30. Hick AC, Delmarcelle AS, Bouquet M, et al. Reciprocal epithelial:endothelial paracrine interactions during thyroid development govern follicular organization and C-cells differentiation. *Dev Biol*. 2013;381(1):227-240. doi:10.1016/j.ydbio.2013.04.022

31. Ishitobi H, Wakamatsu A, Liu F, et al. Molecular basis for Flk1 expression in hemato-cardiovascular progenitors in the mouse. *Development*. 2011;138(24):5357-5368. doi:10.1242/dev.065565

32. Ema M, Takahashi S, Rossant J. Deletion of the selection cassette, but not cis-acting elements, in targeted Flk1-lacZ allele reveals Flk1 expression in multipotent mesodermal progenitors. *Blood*. 2006;107(1):111-117. doi:10.1182/blood-2005-05-1970

33. Hoang T, Lambert JA, Martin R. SCL/TAL1 in Hematopoiesis and Cellular Reprogramming. *Curr Top Dev Biol*. 2016;118:163-204. doi:10.1016/bs.ctdb.2016.01.004

34. Carmeliet P. Mechanisms of angiogenesis and arteriogenesis. *Nat Med*. 2000;6(4):389-

395. doi:10.1038/74651

35. Lewis, Margaret Reed, and Warren H. Lewis. The contraction of smooth muscle cells in tissue cultures. *American Journal of Physiology-Legacy Content*. Published online 1917. https://journals.physiology.org/doi/pdf/10.1152/ajplegacy.1917.44.1.67

36. Pierce ME. The amnion of the chick as an independent effector. *J Exp Zool*. 1933;65(3):443-473. doi:10.1002/jez.1400650307

37. Cuthbert AW. An acetylcholine-like substance and cholinesterase in the smooth muscle of the chick amnion. *J Physiol*. 1963;166:284-295. doi:10.1113/jphysiol.1963.sp007105

38. Becht E, McInnes L, Healy J, et al. Dimensionality reduction for visualizing single-cell data using UMAP. *Nat Biotechnol*. 2018;37(1):38-44. doi:10.1038/nbt.4314

39. Dady A, Blavet C, Duband JL. Timing and kinetics of E- to N-cadherin switch during neurulation in the avian embryo. *Dev Dyn*. 2012;241(8):1333-1349. doi:10.1002/dvdy.23813

40. Trzpis M, McLaughlin PMJ, de Leij LMFH, Harmsen MC. Epithelial cell adhesion molecule: more than a carcinoma marker and adhesion molecule. *Am J Pathol*. 2007;171(2):386-395. doi:10.2353/ajpath.2007.070152

41. Greenbaum A, Hsu YMS, Day RB, et al. CXCL12 in early mesenchymal progenitors is required for haematopoietic stem-cell maintenance. *Nature*. 2013;495(7440):227-230. doi:10.1038/nature11926

42. Alimperti S, Andreadis ST. CDH2 and CDH11 act as regulators of stem cell fate decisions. *Stem Cell Res*. 2015;14(3):270-282. doi:10.1016/j.scr.2015.02.002

43. Oike Y, Yasunaga K, Suda T. Angiopoietin-related/angiopoietin-like proteins regulate angiogenesis. *Int J Hematol*. 2004;80(1):21-28. doi:10.1532/ijh97.04034

44. La Manno G, Soldatov R, Zeisel A, et al. RNA velocity of single cells. *Nature*. 2018;560(7719):494-498. doi:10.1038/s41586-018-0414-6

45. Cao J, Spielmann M, Qiu X, et al. The single-cell transcriptional landscape of mammalian organogenesis. *Nature*. 2019;566(7745):496-502. doi:10.1038/s41586-019-0969-x

46. Dyer LA, Kirby ML. The role of secondary heart field in cardiac development. *Dev Biol*. 2009;336(2):137-144. doi:10.1016/j.ydbio.2009.10.009

47. Abu-Issa R. Heart fields: spatial polarity and temporal dynamics. *Anat Rec* . 2014;297(2):175-182. doi:10.1002/ar.22831

48. Bressan M, Liu G, Mikawa T. Early mesodermal cues assign avian cardiac pacemaker fate potential in a tertiary heart field. *Science*. 2013;340(6133):744-748. doi:10.1126/science.1232877

49. Kelly RG. The second heart field. *Curr Top Dev Biol*. 2012;100:33-65. doi:10.1016/B978-0-12-387786-4.00002-6

50. Cai CL, Liang X, Shi Y, et al. Isl1 identifies a cardiac progenitor population that proliferates prior to differentiation and contributes a majority of cells to the heart. *Dev Cell*. 2003;5(6):877-889. doi:10.1016/s1534-5807(03)00363-0

51. Watanabe Y, Miyagawa-Tomita S, Vincent SD, Kelly RG, Moon AM, Buckingham ME. Role of mesodermal FGF8 and FGF10 overlaps in the development of the arterial pole of the heart and pharyngeal arch arteries. *Circ Res*. 2010;106(3):495-503. doi:10.1161/CIRCRESAHA.109.201665

52. Kelly RG, Brown NA, Buckingham ME. The arterial pole of the mouse heart forms from Fgf10-expressing cells in pharyngeal mesoderm. *Dev Cell*. 2001;1(3):435-440. doi:10.1016/s1534-5807(01)00040-5

53. Kudo M, Ukeshima A, Fujimoto T. The Sites of Intra-embryonic Haemopoiesis Prior to the Hepatic Haemopoiesis in the Chick. *Arch Histol Cytol*. 1989;52(4):355-360. doi:10.1679/aohc.52.355

54. Ukeshima A, Kudo M. The sites and expansion of intra-embryonic blood islands in the early chick embryo. *Okajimas Folia Anat Jpn*. 1993;70(4):165-169. doi:10.2535/ofaj1936.70.4_165

55. Nakano H, Liu X, Arshi A, et al. Haemogenic endocardium contributes to transient definitive haematopoiesis. *Nat Commun*. 2013;4:1564. doi:10.1038/ncomms2569

56. Yzaguirre AD, Speck NA. Insights into blood cell formation from hemogenic endothelium in lesser-known anatomic sites. *Dev Dyn*. 2016;245(10):1011-1028. doi:10.1002/dvdy.24430

57. Li Z, Lan Y, He W, et al. Mouse embryonic head as a site for hematopoietic stem cell development. *Cell Stem Cell*. 2012;11(5):663-675. doi:10.1016/j.stem.2012.07.004

58. Shigeta A, Huang V, Zuo J, et al. Endocardially Derived Macrophages Are Essential for Valvular Remodeling. *Dev Cell*. 2019;48(5):617-630.e3. doi:10.1016/j.devcel.2019.01.021

59. Sheng G, Foley AC. Diversification and conservation of the extraembryonic tissues in mediating nutrient uptake during amniote development. *Ann N Y Acad Sci*. 2012;1271:97-103. doi:10.1111/j.1749-6632.2012.06726.x

60. Dobreva MP, Abon Escalona V, Lawson KA, et al. Amniotic ectoderm expansion in mouse occurs via distinct modes and requires SMAD5-mediated signalling. *Development*. 2018;145(13). doi:10.1242/dev.157222

61. Zhang Q, Carlin D, Zhu F, et al. Unveiling Complexity and Multipotentiality of Early Heart Fields. *Circ Res*. 2021;129(4):474-487. doi:10.1161/CIRCRESAHA.121.318943

62. Liang S, Johansson E, Barila G, Altschuler DL, Fagman H, Nilsson M. A branching morphogenesis program governs embryonic growth of the thyroid gland. *Development*. 2018;145(2). doi:10.1242/dev.146829

63. Yamasaki M. Comparative anatomical studies on the thyroid and thymic arteries. IV. Rabbit (Oryctolagus cuniculus). *J Anat*. 1996;188 (Pt 3):557-564.

https://www.ncbi.nlm.nih.gov/pubmed/8763473

64. Gans C, Northcutt RG. Neural crest and the origin of vertebrates: a new head. *Science*. 1983;220(4594):268-273. doi:10.1126/science.220.4594.268

65. Giles PB, Candy CL, Fleming PA, Owens RW, Scott Argraves W, Drake CJ. VEGF directs newly gastrulated mesoderm to the endothelial lineage. *Dev Biol*. 2005;279(1):169-178. doi:10.1016/j.ydbio.2004.12.011

66. Yvernogeau L, Gautier R, Khoury H, et al. An in vitro model of hemogenic endothelium commitment and hematopoietic production. *Development*. 2016;143(8):1302-1312. doi:10.1242/dev.126714

67. Hao Y, Hao S, Andersen-Nissen E, et al. Integrated analysis of multimodal single-cell data. *Cell*. 2021;184(13):3573-3587.e29. doi:10.1016/j.cell.2021.04.048

Figure Legends

Figure 1 iASCs in the heart, infrahyoid muscles and thyroid gland of HH34-35 AS chimeras. (A-D) Images of QCPN immunostaining in transverse sections of the heart. QCPN-positive cells (brown) are considered iASCs of quail origin. (B) and (D) are higher magnifications of boxes in (A) and (C), respectively. (E-H) Immunostained images of a section adjacent to the box indicated in (D). mCherry signals indicate iASCs. MF20 and DAPI indicate cardiomyocytes and nuclei, respectively. Arrowheads and arrows indicate MF20 positive and negative iASCs, respectively. (I-L) Immunostained coronary septal branch in a section adjacent to the box indicated in (D). Arrowheads indicate αSMA and mCherry doble positive iASCs. (M) QCPN immunostaining in transverse sections of the cervical tissue. (N) Magnified image of the box in (M). (O-R) Immunostained images of a section adjacent to (N). mCherry and QH1 indicate iASCs and quail-derived angioblasts/vascular endothelial cells, respectively. TTF1 stains the epithelium of trachea. Arrowheads and arrows indicate QH-positive and -negative iASCs, respectively. (S) QCPN immunostaining in a transverse section of the thyroid gland. (T) Magnified image of the box in (S). (U-X) Immunostained images of a section adjacent to the box in (T). TTF1 stains the thyroid parenchyma. Scale bars: 1mm for (A, C, M and S), 50μm for other images. RA, right ventricle; LV, left ventricle; RV, right ventricle; pa, pulmonary artery; av, aortic valve; sb, coronary septal branch; es, esophagus; ca, carotid artery; tr, trachea; ifh, infrahyoid muscle; jv, jugular vein; ng, ganglion; pt, parathyroid; thy, thyroid gland.

Figure 2 iASCs integrated into the peri- and intra-thyroid vasculature. Immunostained or angiographic images of AS chimeras with QH1 for quail-derived angioblasts/vascular endothelial cells and TTF1 for the thyroid parenchyma at HH27 (A-D), HH30 (E-H), and HH32 (I-L). Arrowheads in (A) and (E) indicate QH1-positive iASCs, which line vessel

lumens visualized by ink (D, H). Arrowheads in (I) indicates QH1 and mCherry double positive iASCs in the thyroid. Note that QH1 antibody reacted with hematopoietic cells as a background, as shown in (J). Scale bars=100μm. thy, thyroid; TW, thoracic wall.

Figure 3 FGF and signals from the thyroid gland are required for endothelial differentiation of ASCs. (A) Schematic illustration of co-culture experiment. (B, C) QH1- and DAPI-stained images. (a-d) Quail AS grafts are co-cultured with HH30 or HH35 chick thyroid explants in DMEM with 1% FBS in the absence (a and b; n=12 for HH30, n=3 for HH35), or the presence (c and d; n=13 for HH30, n=4 for HH35) of FGF2 (20ng/ml). Arrowheads indicates QH1-positive endothelial cells. (e-h) Quail AS grafts are co-cultured with HH30 or HH35 chick parathyroid and thymus explants in DMEM with 1%FBS in the absence (e and f; n=3 for HH30, n=3 for HH35), or the presence (g and h; n=4 for HH30, n=3 for HH35) of FGF2 (20ng/ml). Asterisks indicate remnant organ grafts. Scale bars=200μm. (D) Quantitative comparison of QH1-positive areas. "para" indicates parathyroid and thymus. Box plot shows the median and quartiles 1 and 3 of the ratio of QH1 positive- to DAPI positive- areas of each group. *P<0.05, **P<0.0001.

Figure 4 Sequential FGF and VEGF signals promote vascular endothelial differentiation of ASCs. (A) Comparison of *VEGFA* mRNA levels between the thyroid (thy) and parathyroid/thymus (para) of HH35 chick embryos (n=3) by quantitative RT-PCR (qPCR). *P <0.05. (B) Time-series changes (6, 12, 24, 48, 72h) in *KDR*/*VEGFR2* mRNA levels by qPCR. Gray and black lines indicate changes in the average values of control and FGF2-treated samples, respectively, from 3 independent experiments. Error bars indicate S.E. (C) Appearance of QH1 positive endothelial cells around 48h-cultured quail ASC explants in DMEM with 1% FBS in the absence (a and b; n=11), or the presence of 50ng/ml VEGF-A (c

and d; n=10), 20ng/ml FGF2 (e and f; n=20) or both with an interval of 24 hours (VEGF-A after FGF2) (g and h; n=31). Asterisks indicate ectodermal tissues. Scale bars = 200μm. (D) Box plot shows the median and quartiles 1 and 3 of the ratio of QH1 positive- to DAPI positive- areas of each group (control, n=8; VEGF-A, n=10; FGF2, n=10; FGF + VEGF-A, n=10). *P <0.05, **P <0.005.

Figure 5 Effects of FGF and/or VEGF on the expression levels of endothelial differentiation-related genes. (A-D) qPCR analysis of 48h-cultured quail ASCs under conditions as in Figure 4C for mRNA levels of *VEGFR2* (A), *TAL1* (B), *LMO2* (C) and *CDH5* (D). Data were obtained from 5 independent experiments. Error bars indicate S.E. *P < 0.0125. (E-H) The expression levels of *KDR/VEGFR2* and FGF receptors before (culture 0h) and after (FGF24h + VEGF24h) endothelial differentiation of ASCs. Error bars indicate S.E. *P < 0.05, **P < 0.01.

Figure 6 Mature amnion cells do not respond to FGF and VEGF signaling. (A) HH30 quail embryo which is completely wrapped in amniotic membrane (arrow). (B-I) QH1- and DAPI-stained images of HH30 amnion grafts are cultured under conditions as follows: Control 48h, n=7 (B and C); control 24h + 50ng/ml VEGF-A 24h, n=5 (D and E); 20ng/ml FGF2 48h, n=5 (F and G); FGF2 24h + VEGF-A 24h, n=7 (H and I). Asterisks indicate ectodermal tissues. Scale bars = 200μm

Figure 7 Single-cell RNA sequence (scRNA-seq) of HH10 chick ASCs reveals the existence of vascular endothelial progenitor-like cells in the AS even before intraembryonic translocation. (A) Schematic illustration of single-cell preparation. Both ectodermal (ect) and somatic mesoderm (Som-mes) cells were collected from HH10 chick somatopleural tissues.

(B) scRNA-seq data of all ASCs (89 cells) are displayed as plots on UMAP with different colours representing different clusters. (C) The heatmap shows top 50 differentially expressed genes (DEGs) sorted by log2 fold change between clusters detected by Seurat FindAllMarkers function. The heatmap is coloured according to the Z scores of the average expression values in each cluster. Yellow and purple represent high and low expression levels, respectively. (D) The number of feature RNA (nFeature RNA) and expression levels of some genes of interest on the UMAP. Each plot is coloured according to the Z score of the expression value.

Figure 8 FGF and VEGF receptors expression dynamics along pseudotime. (A) UMAP with a dataset of 75 ASCs from which low-quality ASCs are excluded (cells in cluster 2 shown in Fig. 7B). The cluster numbers correspond to those in Fig. 7B. The clusters are clearly divided into two major populations: the ectoderm (clusters 0 and 9) and mesoderm (clusters 1, 3, 4 and 6) components. (B) RNA velocity based on UMAP. Arrows indicate local average velocity on a regular grid vector field. (C) The mesoderm component in (A) is extracted. (D) Pseudotime values were calculated and plotted. The starting point of the pseudotime is set arbitrarily by referring to the result of velocity shown in (B). (E) Trajectory mapping of the mesoderm component shows some stratification between cell states along the pseudotime, with high expression of FGF receptors at the early stage (a-c) and VEGF receptors at the late stage (d-f). The colour of each plot corresponds to the colour shown in (C).

Figure 9 Presumptive model of the process by which ASCs or iASCs differentiate into the thyroid vascular endothelial cells. scRNA-seq data reveals the existence of VEGFR2-positive cells in the AS before entering the embryo. After migrating into the embryo, FGF signaling from the surrounding mesenchymal cells upregulates VEGFR2 expression in iASCs to be

incorporated into pharyngeal vasculature through vasculogenesis. Then, VEGF signaling from the thyroid further accelerates the maturation and iASCs migrate into the thyroid by angiogenesis.

Table

Primers used for qPCR: q, quail: c, chick

Gene	Orientation	Sequence	Product size
q*VEGFR2*	Forward	ACAAGTATGGCTCAACGCAGA	132
	Reverse	GATTGGCTCCCAGGCGAACTTT	
q*TAL1*	Forward	CCATCGGCAGCGGGTTCTTC	128
	Reverse	GCGGCGGACCACCTTCGTGT	
q*LMO2*	Forward	GACCAATACTGGCACGAGGA	135
	Reverse	ATCTTGGCCAAAGAGCCTGA	
q*CDH5*	Forward	ACCACATCACGTTGGCAAGCTCAC	113
	Reverse	TGTCGCCATCGTACCCTTGCACT	
q*GAPDH*	Forward	AGAACATCATCCCAGCGTCCACT	133
	Reverse	CGGCAGGTCAGGTCAACAACAGA	
q*FGFR1*	Forward	TACCCAAAGGTTTCGTTTGC	134
	Reverse	AGTGTGCATAGGCCCCATAG	
q*FGFR2*	Forward	CTACTCGCCTCTCCTCCACT	110
	Reverse	ACCCAGCGTCAGCTTATCTC	
q*FGFR3*	Forward	AATTGGCACGTTCTCGCCTG	119
	Reverse	CACGGTGATGGCCTTGTTTG	
c*VEGFA*	Forward	ACAAACCACCCAGCTTTCAC	117
	Reverse	TCGACTTGCAACGTGAGTCT	
c*GAPDH*	Forward	ATCCCTGAGCTGAATGGGAAG	101
	Reverse	TTGGCTGGTTTCTCCAGACG	

Supplementary Data

Supplementary data 1. Metadata of the single-cell RNA-seq

Supplementary data 2. Differentially expressed genes (DEGs) in each cluster of HH10 ASCs detected by Seurat FindAllMarkers function

Figures

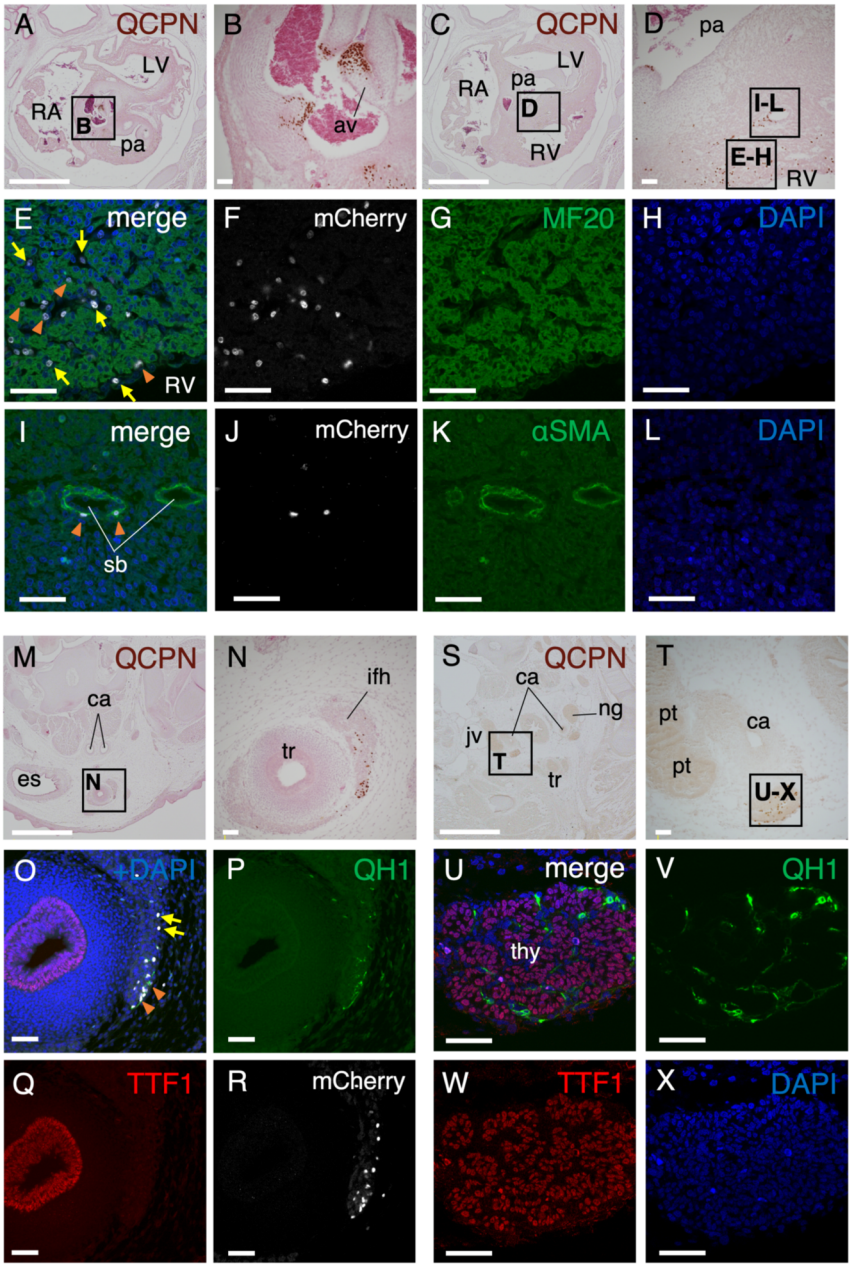

DVDY_532_Slide1.tif

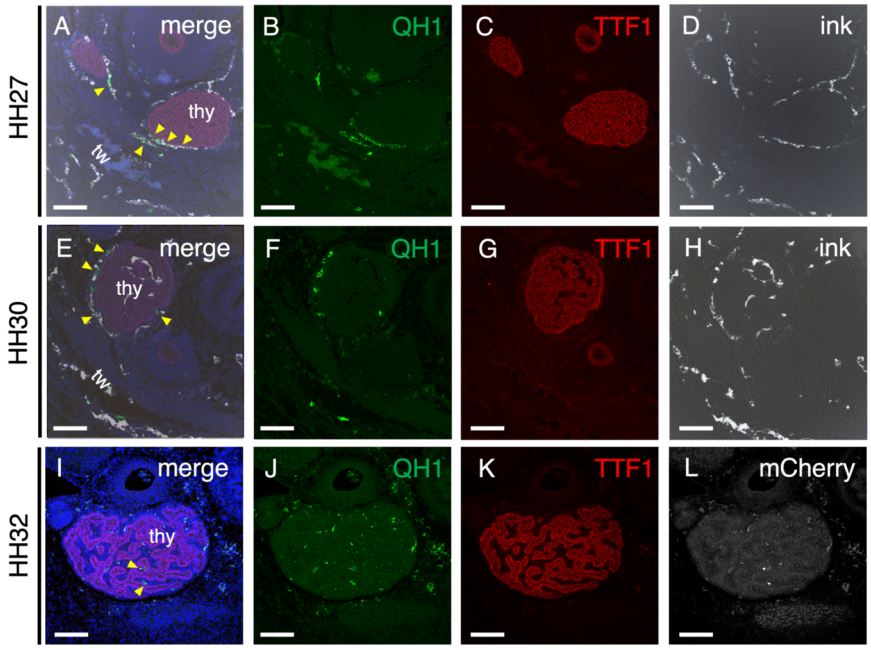

DVDY_532_Slide2.tif

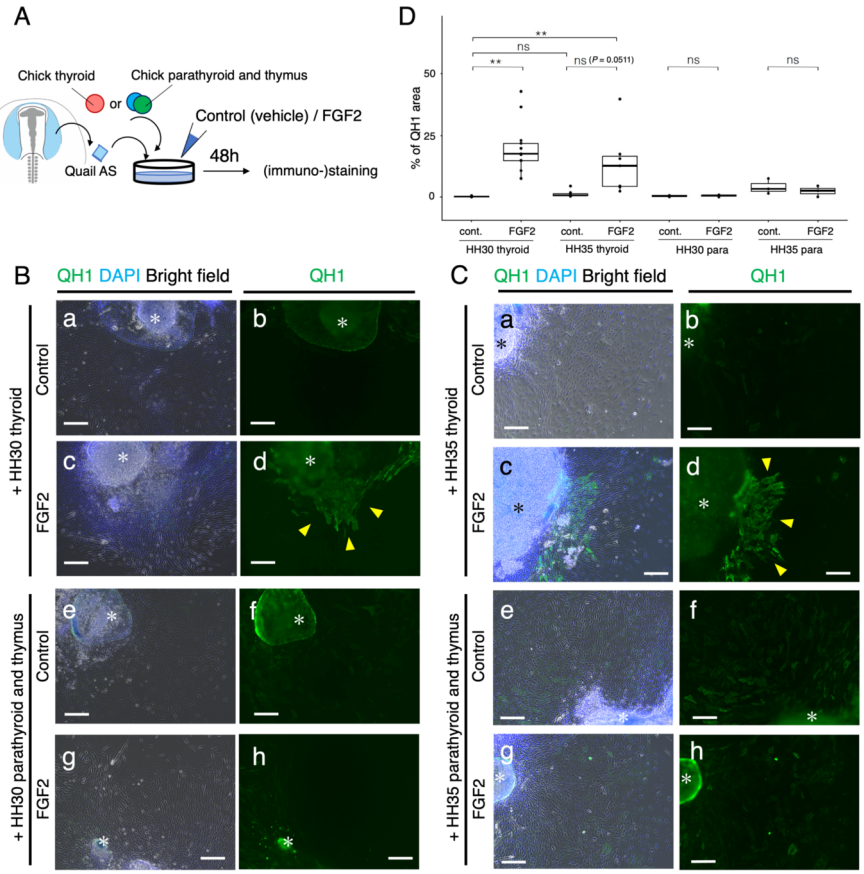

DVDY_532_Slide3.tif

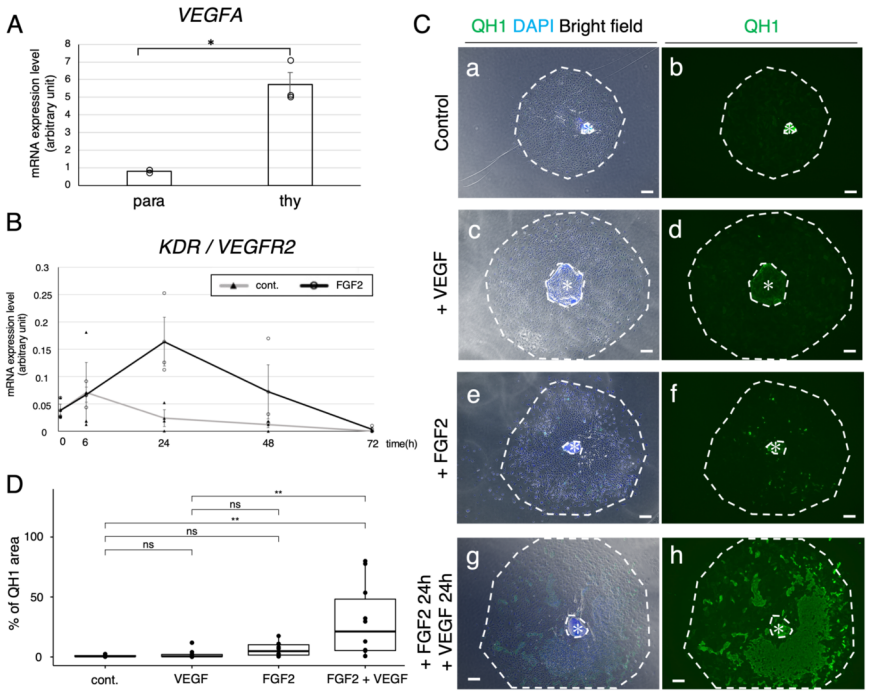

DVDY_532_Slide4.tif

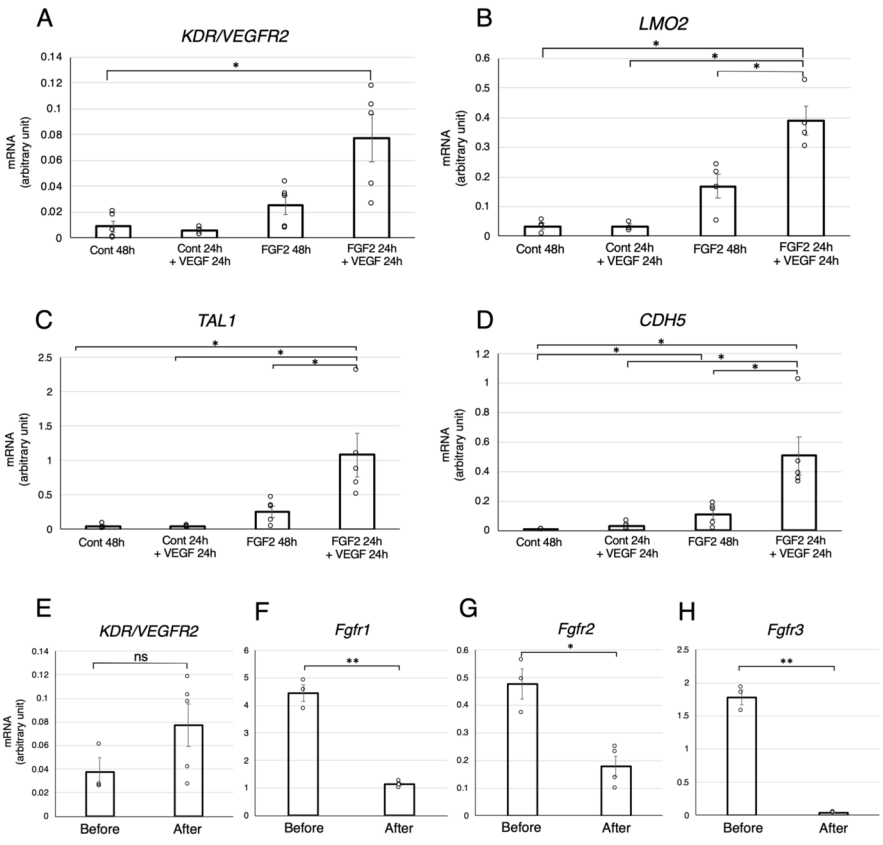

DVDY_532_Slide5.tif

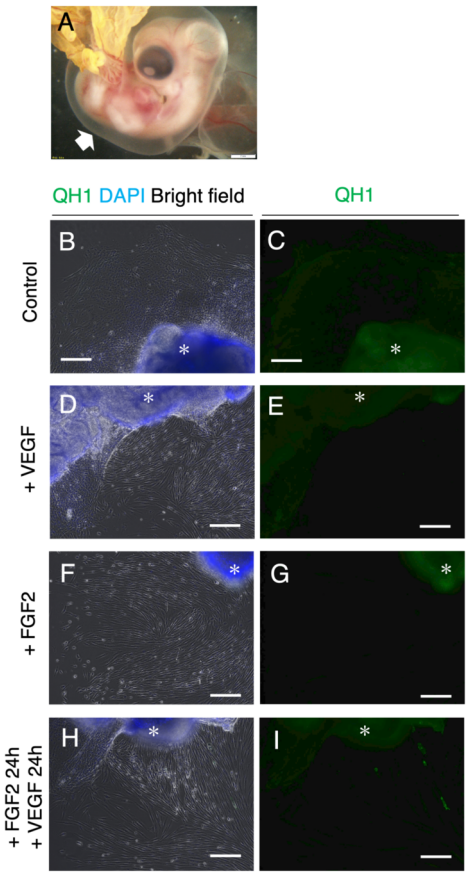

DVDY_532_Fig6.tif

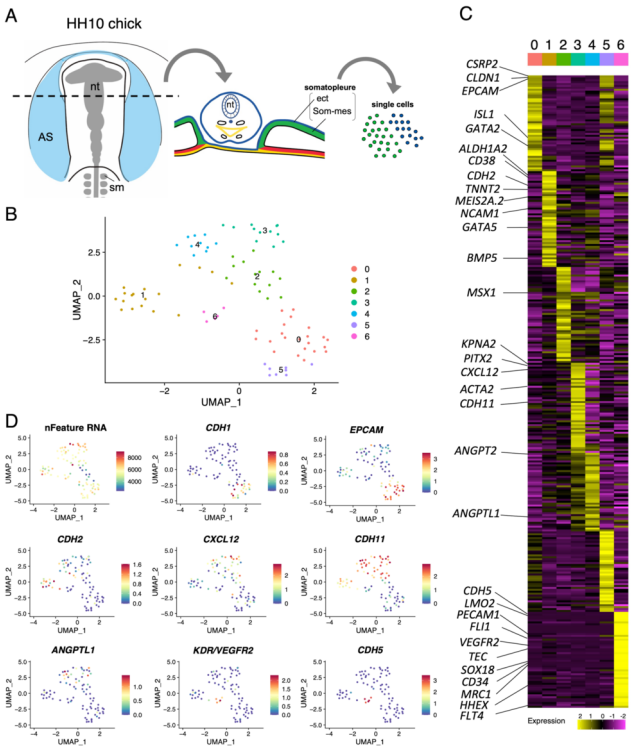

DVDY_532_Slide7.tif

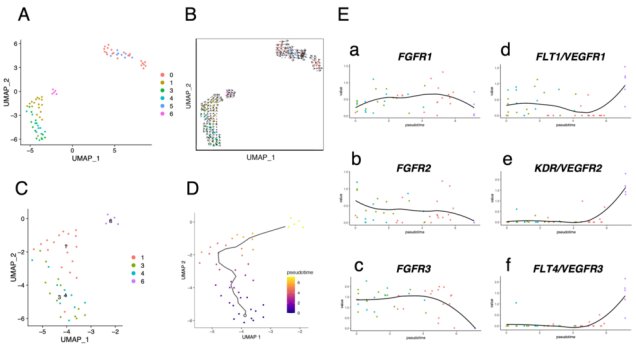

DVDY_532_Slide8.tif

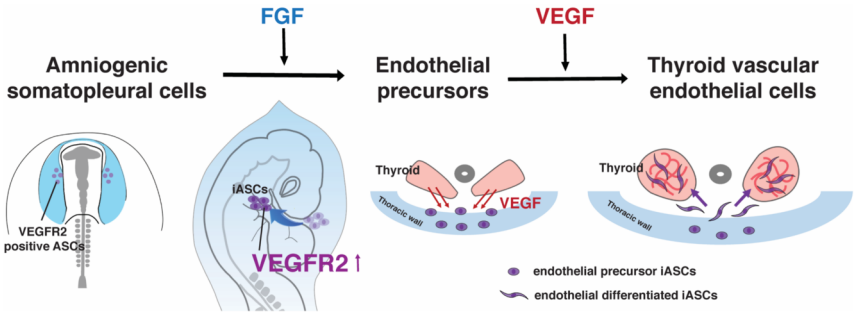

DVDY_532_Slide9.tif